Emission spectroscopy of a microhollow cathode discharge plasma in helium-water gas mixtures

S. Namba, T. Yamasaki, Y. Hane, D. Fukuhara, K. Kozue et al.

Related Articles

Convoluted effect of laser fluence and pulse duration on the property of a nanosecond laser-induced plasma into an argon ambient gas at the atmospheric pressure
J. Appl. Phys. 113, 013304 (2013)

Developing the model of laser ablation by considering the interplay between emission and expansion of aluminum plasma
Phys. Plasmas 20, 013301 (2013)

X-ray emission from a nanosecond-pulse discharge in an inhomogeneous electric field at atmospheric pressure
Phys. Plasmas 19, 123516 (2012)

Radiofrequency plasma antenna generated by femtosecond laser filaments in air
Appl. Phys. Lett. 101, 264106 (2012)

Observations of non-collective x-ray scattering in warm dense carbon plasma
Phys. Plasmas 19, 122709 (2012)

Additional information on J. Appl. Phys.

Journal Homepage: http://jap.aip.org/

Journal Information: http://jap.aip.org/about/about_the_journal

Top downloads: http://jap.aip.org/features/most_downloaded

Information for Authors: http://jap.aip.org/authors

Emission spectroscopy of a microhollow cathode discharge plasma in helium-water gas mixtures

S. Namba,[a] T. Yamasaki, Y. Hane, D. Fukuhara, K. Kozue, and K. Takiyama

Graduate School of Engineering, Hiroshima University, 1-4-1 Kagamiyama, Higashi-Hiroshima, Hiroshima 739-8527, Japan

A dc microhollow cathode discharge (MHCD) plasma was generated inflowing helium gas containing water vapor. The cathode hole diameters were 0.3, 0.7, 1.0, and 2.0 mm, each with a length of 2.0 mm. Emission spectroscopy was carried out to investigate the discharge mode and to determine the plasma parameters. For the 0.3-mm cathode, stable MHCDs in an abnormal glow mode existed at pressures up to 100 kPa, whereas for larger diameters, a plasma was not generated at atmospheric pressure. An analysis of the lineshapes relevant to He at 667.8 nm and to Hα at 656.3 nm implied an electron density and gas temperature of 2×10^{14} cm^{-3} and 1100 K, respectively, for a 100-kPa discharge in the negative glow region. The dependence of the OH band, and Hα intensities on the discharge current exhibited different behaviors. Specifically, the OH spectrum had a maximum intensity at a certain current, while the H atom intensity kept increasing with the discharge current. This observation implies that a high concentration of OH radicals results in quenching, leading to the production of H atoms via the reaction $OH + e^- \rightarrow O + H + e^-$. © *2011 American Institute of Physics*. [doi:10.1063/1.3646551]

I. INTRODUCTION

High-pressure discharges have been attracting a great deal of interest for various applications. For example, atmospheric thermal plasmas can be employed for waste treatment, formation of nanoparticles, thin film deposition, and plasma welding and cutting.[1–3] Atmospheric pressure glow discharges can generate nonequilibrium plasmas that are an alternative means for surface treatments, optical sources, and detoxification of gaseous pollutants.[4–6]

Paschen's scaling law describing the breakdown voltage V_d as a function of the product of the gas pressure P and the gap distance d requires $Pd \approx 10$ Torr·cm for V_d on the order of several hundreds of volts.[6] Consequently, the value of d should be on the order of 10 μm for atmospheric discharges. To attain a discharge at high pressure, a microhollow cathode discharge (MHCD) has received considerable attention[7–9] because a microplasma with a density above 10^{14} cm^{-3} can be produced due to the peculiar geometric configuration. A MHCD at high pressure provides a favorable environment for excimer light sources, since it is capable of generating a nonequilibrium plasma with a large population of high-energy electrons.[9] Moreover, cold atmospheric plasmas generated by MHCDs can be used for medical and biological applications.[10] A microchemical reactor using a MHCD plasma has also been proposed to efficiently extract hydrogen gas from ammonia, as a promising device for portable fuel applications.[11,12]

The discharge operational mode of a MHCD plasma was investigated by Schoenback *et al.*[7–9] Depending on the discharge current and gas pressure, the discharge operated in four different modes (predischarge mode, hollow cathode mode, abnormal glow discharge mode, and surface discharge mode). In addition, the parameters of the microplasma generated in the hollow cathode could be determined by laser atomic absorption spectroscopy. From an analysis of the line shape broadening, the electron density and gas temperature were deduced to be 5×10^{15} cm^{-3} and 1100 K, respectively, for a discharge using a cathode hole diameter of 0.3 mm at 400 mbar of Ar (Ref. 13). Optical emission spectroscopy was also performed to characterize Ar microplasma operated at a pressure of 500 mbar by Spasojević *et al.*[14] By introducing hydrogen gas as a tracer particle and observing the Hβ line shape, they successfully obtained the electron density of 3.8×10^{14} cm^{-3} and the electric field of 127 kV/cm. A numerical study of the MHCD He plasma was performed by Kothnur *et al.* using a two-dimensional fluid model.[15] They showed that with increasing gas pressure the charged particles were confined to the cathode opening. Moreover, the electron density, temperature, and gas density of the microplasma were on the order of 10^{14} cm^{-3}, 10 eV, and 1000 K, respectively, for a cathode with a 0.2-mm-diameter opening at a He gas pressure of 1000 Torr and discharge current of 2.7 mA. The calculated plasma parameters were consistent with the experimental data.

Currently, the use of MHCD plasmas for the remediation of indoor environments is being pursued, such as the treatment of microbial contaminants. The present study focuses on production and quenching processes relevant to H atoms and OH radicals decomposed by a MHCD device from ambient water in air, which are thought to play an important role in deactivation of harmful biological macromolecules.[16] Intense atomic and molecular spectra from nitrogen and oxygen make it difficult to observe the weak H and OH emissions. In general, a high discharge voltage is necessary to generate a stable plasma in air, but the introduction of He gas improves the

stability of the plasma at high pressures for reasonable discharge voltages. In order to investigate the processes associated with H_2O, a MHCD operating in a helium and water vapor gas mixture are investigated spectroscopically in this paper.

Cathode diameters of 0.3 to 2.0 mm are used to generate the microplasmas. Emission spectroscopy shows that for a 0.3-mm cathode, a stable MHCD plasma is produced in the hole at atmospheric pressure. It also reveals that the ionization and excitation are dominated by collisional or photon induced processes, depending on the gas pressure and diameter of the cathode opening. The electron density and gas temperature are derived from an analysis of the lineshapes of He neutral and H emission spectra. The dependence of the OH radical emission intensity on the discharge current is also examined to investigate its production and quenching processes.

II. EXPERIMENTAL SETUP

Figure 1 shows (a) a photograph, and Fig. 1(b) a schematic diagram of the MHCD plasma device. The cathode and anode were both made of brass, and ceramic disks were used to electrically insulate the electrodes. Four cathode disks had inner hole diameters of $D = 0.3$, 0.7, 1.0, and 2.0 mm, all with lengths of $L = 2.0$ mm. The respective anodes and ceramic disks had the same inner diameters as the cathode openings. The MHCD plasma device was installed in a vacuum chamber and He gas with a flow rate of 1.0 L/min was fed into it. Water vapor was introduced into the He carrier gas by passage through a steam vessel. The direct current discharge was operated at sustaining voltages of 180–400 V, currents of 2–50 mA, and gas pressures of 0.6–100 kPa.

The MHCD plasmas generated in the cathode opening were observed using a high-resolution visible spectrometer

FIG. 1. (Color online) (a) Photograph and (b) schematic diagram of the MHCD device. The cathodes had opening diameters of $D = 0.3$, 0.7, 1.0, and 2.0 mm with a length of 2.0 mm. The anode and cathode were electrically separated by an insulator.

with a focal length of 1 m and a grating of 2400 grooves/mm. The detectors were a charge-coupled device (CCD) camera and a photomultiplier tube (PMT). Since the plasma region was as small as 0.3 mm, the emission image was magnified five-fold using a quartz lens. The spatial resolution was approximately 5 μm. We observed three emission spectra: Hα ($n = 3 \to 2$ at 656.3 nm), He I ($2^1p - 3^1d$ at 667.8 nm), and OH band (A–X transition around 309 nm). For the OH spectra, the resolution was not high enough to observe the fine structure arising from the rotational transitions. Consequently, second-order light from the fundamental emission was measured to improve the spectral resolution. The resolution in the Hα and He I 667-nm wavelength region was determined by measuring a HeNe laser at 632.8 nm. Assuming that the line profile has a Gaussian distribution, the instrumental width [full width at half maximum (FWHM)] was determined to be $\Delta\lambda_{instrum} = 9$ pm for the CCD and $\Delta\lambda_{instrum} = 7$ pm for the PMT. The spectral sensitivity of the whole optical system was calibrated using standard lamps (tungsten ribbon and xenon discharge). The CCD images were measured through an entrance slit of 2.5 mm, enabling observation of two-dimensional spectral images.

III. SPECTRAL LINESHAPES DUE TO BROADENING EFFECTS

Spectral lines are broadened due to the instrumental width, Doppler broadening, pressure broadening, and Stark broadening, from which the plasma parameters can be derived. Because a detailed description of these effects is available from many sources, they are only briefly summarized here.

When the velocity distribution is Maxwell-Boltzmann, the FWHM for Doppler broadening is[17,18]

$$\Delta\lambda_D(\text{nm}) = 7.16 \times 10^{-7}\lambda_0\sqrt{\frac{T_g}{M}}, \qquad (1)$$

where λ_0 is the peak wavelength (in nm), T_g is the gas temperature (in K), and M is the atomic mass (in amu).

Pressure broadening has two origins: resonance broadening of the He I 2p–3d transition and van der Waals broadening for Hα. Resonance broadening arises from interactions between neutral atoms of the same kind. It occurs for allowed transitions involving a level that is dipole-coupled to the ground state. The linewidth is described by the Lorentzian profile[18–20]

$$\Delta\lambda_R(\text{nm}) = 8.61 \times 10^{-28}\sqrt{\frac{g_1}{g_2}}\lambda_0^2\lambda_R f_R N_a, \qquad (2)$$

where g_1 and g_2 are the degeneracies of the lower and upper states of the transition (1^1S–2^1P), respectively, λ_R and f_R are the wavelength (in nm) and absorption oscillator strength of the resonance line, respectively, and N_a (in cm^{-3}) is the density of perturber particles (i.e., the He gas density). For He I at 667.8 nm, Eq. (2) becomes $\Delta\lambda_R(\text{nm}) = 0.26 \times P(\text{kPa})/T_g(\text{K})$ where P is the gas pressure. On the other hand, short-range interactions between the radiator and other atoms or
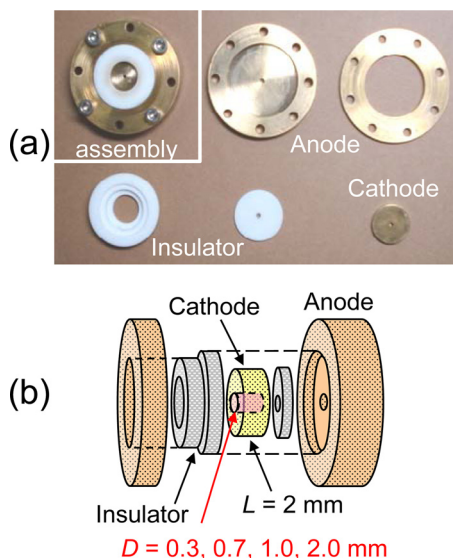
molecules give rise to van der Waals broadening whose FWHM is[18–20]

$$\Delta\lambda_V(\text{nm}) = 8.18 \times 10^{-5}\lambda_0^2(\bar{\alpha}\overline{R^2})^{2/5}\left(\frac{T_g}{\mu}\right)^{3/10} N_a, \quad (3)$$

where $\bar{\alpha}$ is the mean atomic polarizability of the perturbers, μ is the reduced mass (in amu), and $\overline{R^2}$ is the difference in the squares of the coordinate vectors (in units of a_0) of the upper and lower levels, as given by

$$\overline{R^2} = \overline{R_U^2} - \overline{R_L^2} \quad (4)$$

and

$$\overline{R_j^2} = n_j^{*2}/2\left[5n_j^{*2} + 1 - 3l_i(l_i + 1)\right], \quad (5)$$

where n_j^* is the effective quantum number and l_i is the angular quantum number. For Hα, Eq. (3) becomes $\Delta\lambda_V(\text{nm}) = 0.019 \times P(\text{kPa})/T_g^{0.7}(\text{K})$.

The Stark effect in high-density plasmas also broadens the line shape.[21] Gigosos *et al.* calculated the line shapes of Balmer series for various conditions, in which ion dynamic effect for non-equilibrium condition was taken into account.[22] For Hα spectrum, the Stark width obtained by fitting their results is expressed by the following function,

$$\Delta\lambda_S^H(\text{nm}) = 2.05 \times 10^{-11} n_e^{0.63}. \quad (6)$$

For He I at 667.8 nm, the Stark width is approximately given by[16–18]

$$\begin{aligned}\Delta\lambda_S^{He}(\text{nm}) = 2 \times \Big[&1 + 1.75 \times 10^{-4} n_e^{1/4}\alpha \\ &\times\left(1 - 0.068 n_e^{1/6}T_e^{-1/2}\right)\Big]10^{-16}w_e n_e,\end{aligned} \quad (7)$$

where α and w_e are the ion broadening parameter and the FWHM of the broadening due to electron impacts, as tabulated in Ref. 21. The electron density can be derived from the spectral widths in Eqs. (6) and (7).

The observed intensity distribution is approximated by a Voigt profile that is the convolution of a Gaussian (due to the instrumental and Doppler broadenings) and a Lorentzian (due to the resonance or van der Waals and the Stark broadenings). For the Gaussian, the total FWHM is

$$\Delta\lambda_G = \sqrt{\Delta\lambda_{\text{instrum}}^2 + \Delta\lambda_D^2}, \quad (8)$$

whereas for the Lorentzian it is

$$\Delta\lambda_L = \Delta\lambda_V + \Delta\lambda_S^H \quad \text{for Hα} \quad (9)$$

and

$$\Delta\lambda_L = \Delta\lambda_R + \Delta\lambda_S^{He} \quad \text{for He.} \quad (10)$$

By fitting the experimental data with a Voigt profile, the Gaussian and Lorentzian components can be obtained.

IV. RESULTS AND DISCUSSION

A. Two-dimensional spatial images

Figure 2 shows two-dimensional spatial images of (a) He I at 667.8 nm and (b) Hα spectra for He gas pressures ranging from 0.7 to 21 kPa. The discharge current was 20 mA and its voltage was approximately 225 V. The diameter of the cathode opening ($D = 1.0$ mm) is indicated by the dotted circles in the leftmost panels. The size of the horizontal emission was limited by the entrance slit of the spectrometer. The slight distortion from circularity is due to the astigmatism of the spectrometer. Above 21 kPa, a plasma was not produced because higher discharge voltages are required to ignite gaseous breakdown. At pressures below 6 kPa, both the H and He emissions were most intense at the cathode center, indicating that ionization occurs due to a pendulum motion of the electrons around the virtual anode located along the central axis. At pressures of 7 and 21 kPa, however, the 2D emission of He at 667.8 nm showed a hollow structure. With increasing gas pressure, the ring-shaped emission region approached the cathode electrode and became thinner. This phenomenon can be interpreted in terms of the mean free path of an inelastic collision. Electrons accelerated in the cathode sheath collide with neutral atoms, resulting in excitation and ionization. The higher the atomic density, the more frequently collisions occur and thus the mean free path becomes shorter. The emission region is therefore localized near the inner wall of the cathode.[9,15] In contrast to that behavior of the He spectrum, Hα was predominantly emitted at the center for all gas pressures, although weak ring emission was also observed. This result suggests that in the cathode region the population channels into H level $n = 3$ and He level 3^1d are similar, whereas around the cathode axis an alternative mechanism responsible for population inflow into H $n = 3$ is involved. Dissociative recombination such as $H_2O^+ + e^- \rightarrow H^*(n = 3) + OH$ might be involved, owing to the relatively low temperature plasma in the center.[15]

For the $D = 0.3$ mm cathode, a stable discharge inside the cathode opening occurred for gas pressures up to atmospheric. Figure 3 shows two-dimensional images of (a) He I and (b) Hα at a current of 20 mA. The current-voltage characteristics indicated that the discharge was operating in an abnormal glow discharge mode. With increasing gas pressure, the plasma radius decreased. Even at 100 kPa, no ring-shaped emission was observed around the cathode edge, implying that photoionization arising from vacuum UV and
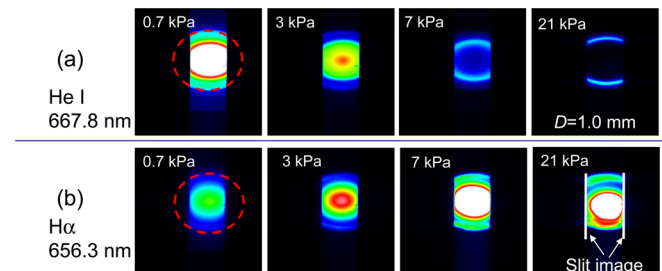

FIG. 2. (Color online) Two-dimensional emission images of (a) He I at 667.8 nm and (b) Hα at 656.3 nm for He gas pressures between 0.7 and 21 kPa. The observations were performed using a cathode opening of $D = 1.0$ mm at a discharge current of 20 mA and voltage of 225 V.
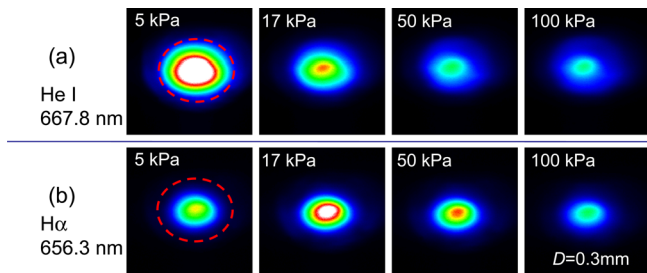
FIG. 3. (Color online) Emission images of (a) He I at 667.8 nm and (b) Hα at 656.3 nm for a $D = 0.3$ mm cathode at a discharge current of 20 mA and voltage of 250 V.

UV lights emitted from the cathode surface rather than electron collisional effects are likely playing a key role in the generation of plasmas at high pressures.[9]

B. Determination of T_e and n_e

The lineshapes of He I at 667.8 nm and of Hα at 656.3 nm were measured. Figure 4 shows the results obtained using the CCD camera for a 0.3-mm cathode diameter, discharge current of 20 mA, and slit width of 30 μm. The observation region was approximately 15 μm around the cathode center. With increasing gas pressure, the He I and Hα spectra broadened due to the resonance and van der Waals effects, respectively. Moreover, Stark broadening due to charged particles also influenced the lineshapes in high-density plasmas. Similar dependence of the intensity distribution on the gas pressure was observed for other cathodes.
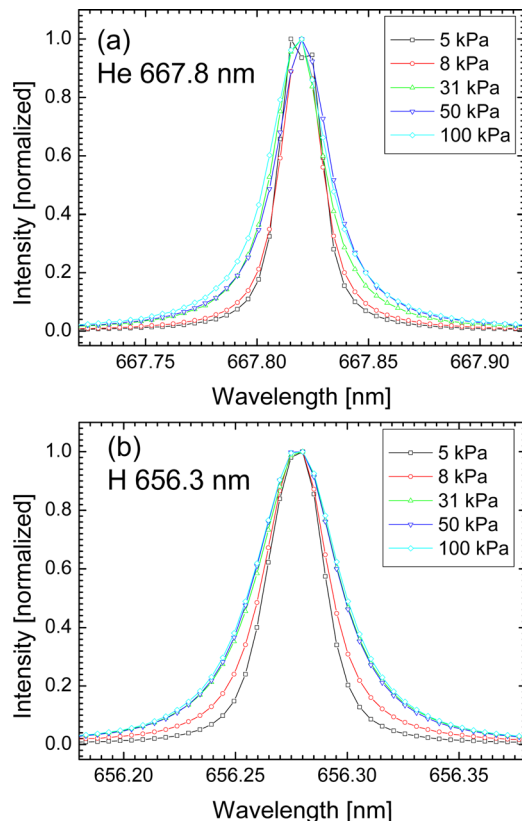

FIG. 4. (Color online) Line profile of (a) He I at 667.8 nm and (b) Hα at 656.3 nm as a function of the gas pressure for a cathode of 0.3-mm diameter and a current of 20 mA.
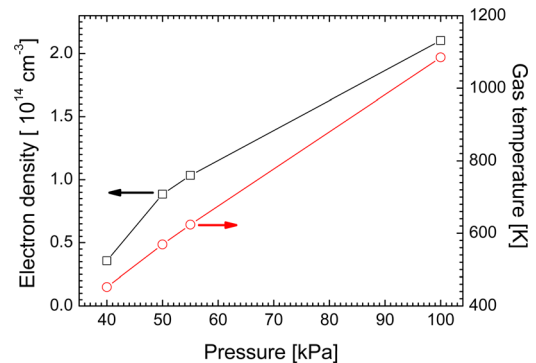

FIG. 5. (Color online) Electron density and gas temperature derived from the line shape analysis for various gas pressures (for a 0.3-mm cathode and a current of 20 mA).

The electron density and gas temperature for a 0.3-mm-diameter cathode were derived from an analysis of the linewidths of the He and H spectra as follows. A value for the gas temperature T_g of the plasma was estimated and used to calculate the Doppler broadening width $\Delta\lambda_D$ from Eq. (1). The total Gaussian width $\Delta\lambda_G$ was then obtained from Eq. (8). By fitting the experimental data with a Voigt function having Gaussian width $\Delta\lambda_G$, the total Lorentzian widths $\Delta\lambda_L$ were obtained from Eqs. (9) and (10) for the Hα and He 667.8-nm spectra, respectively. Estimating a value for the electron density and assuming its temperature to be 10 000 K, Eq. (7) then gives the Stark width for He at 667.8 nm, $\Delta\lambda_S^{He}$, and thereby the resonance broadening width $\Delta\lambda_R$ from Eq. (10). From the measured gas pressure and estimated $\Delta\lambda_R$, the gas temperature T_g was obtained. This *revised* gas temperature was used to calculate $\Delta\lambda_R$ from Eq. (3), and Eq. (9) then gave the Stark width, resulting in a determination of the electron density from Eq. (6). These calculations were then repeated until the results converged. It was confirmed that the electron temperature dependence on the Stark width below 50 000 K was unimportant.[23]

Figure 5 graphs the electron density and gas temperature on the cathode axis at a discharge current of 20 mA as a function of the gas pressure. The density obtained at 100 kPa was as high as $\sim 2 \times 10^{14}$ cm^{-3}, whereas the gas temperature increased from 360 K at 30 kPa to 1085 K at 100 kPa. With increasing pressure, the electrons gain less energy in collisions with neutral atoms and transfer more energy to the gas via elastic collisions, resulting in significant gas heating. Both the density and temperature derived in this study are in
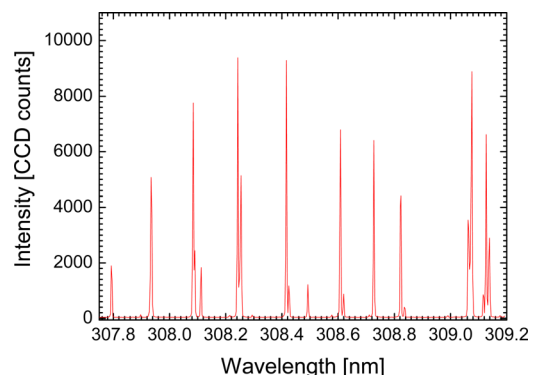

FIG. 6. (Color online) Hydroxyl (OH) band spectra in second order observed for $D = 0.3$ mm at 20 mA and 100 kPa.
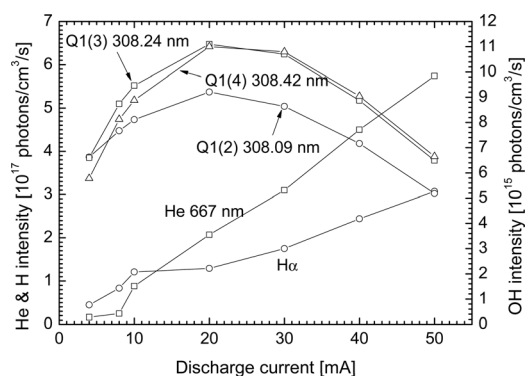
FIG. 7. Absolute emission intensities of the OH A–X transition, He at 667.8 nm, and Hα for the same experimental conditions as in Fig. 6.

good agreement with the experimental[24] and calculated[15] values for a similar experimental setup.

C. OH radical emission

The dissociation of water introduced into the discharge section yields OH radicals and H atoms. Figure 6 indicates the OH (A–X) emission around 308 nm for a 0.3-mm cathode at 20 mA and 100 kPa. Figure 7 shows the OH emission intensity for various discharge currents (for $D = 0.3$ mm at 100 kPa). Three Q-branch emissions are plotted: Q1(2) at 308.09 nm, Q1(3) at 308.24 nm, and Q1(4) at 308.42 nm. The intensity increases with discharge current up to a peak at about 20 mA. With further increase of the current, the intensities decrease. The reason for this decrease is the high concentration of OH radicals at high discharge currents, resulting in the formation of H_2O_2 molecules due to the reaction

$$OH + OH \rightarrow H_2O_2 \qquad (11)$$

and the collisional dissociation by electron impact,

$$OH + e^- \rightarrow O + H + e^-. \qquad (12)$$
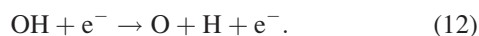
In order to clarify the mechanism underlying the OH emission, the dependence of the He 667-nm and Hα emission intensities on the discharge current was investigated. These results are also presented in Fig. 7. In contrast to the peak in the OH radical emission, both the Hα and He 667.8-nm intensities increased monotonically. Therefore, dissociation quenches the OH radicals. Accordingly, by choosing the optimal discharge current, hydrogen atoms can be produced without further formation of OH radicals.

In order to determine the gas temperature, the line distribution from the spectral simulation code LIFBASE[25] was compared with the experimental results, assuming that the vibrational temperature is equal to the rotational one. With increasing current, the temperature increased from 420 K at 2 mA up to 750 K at 50 mA for $D = 0.3$ mm at 100 kPa, in reasonable agreement with the results obtained from the linewidths.

V. CONCLUSIONS

Microhollow cathode discharge devices having cathode diameters ranging from 0.3 to 2.0 mm were fabricated to generate stable microplasmas at atmospheric pressure. The discharge operated in helium gas containing water vapor and was characterized by optical emission spectroscopy. Two-dimensional imaging showed that for larger diameter cathodes, a plasma was not generated at high gas pressures, but a stable abnormal glow discharge arose for a 0.3-mm cathode even at 100 kPa.

An analysis of the lineshapes of He I at 667.8 nm and of Hα for a 0.3-mm-diameter cathode indicated that with increasing gas pressure the electron density and the gas temperature increased to 2×10^{14} cm^{-3} and 1100 K, respectively, at 100 kPa and 20 mA.

The dependence of the OH and H spectral intensities on the discharge current showed that the number of H atoms increased with the current, while there was an optimum current to generate OH radicals. In addition, the gas temperature was determined by comparing the OH band spectra to those from the LIFBASE simulation code. The temperatures derived from this method were in good agreement with those determined by the line profile analysis.

[1]M. I. Boulos, P. Fauchais, and E. Pfender, *Thermal Plasmas, Fundamental and Applications* (Plenum, New York, 1994).
[2]C. Tendero, C. Tixier, P. Tristant, J. Desmaison, and P. Leprince, Spectrochim. Acta, Part B **61**, 2 (2006).
[3]L. Bárdos and H. Baránková, Thin Solid Films **518**, 6705 (2010).
[4]M. Morea, N. Orange, and M. G. J. Feuilloley, Biotechnol. Adv. **26**, 610 (2008).
[5]J. Reece Roth, "Industrial Plasma Engineering," in *Applications to Nonthermal Plasma Processing* (IOP, Bristol, 2001), Vol. 2.
[6]Yu. P. Raizer, Gas Discharge Physics (Springer, Berlin, 1991).
[7]K. Schoenbach, A. El-Habachi, W. Shi, and M. Ciocca, Plasma Sources Sci. Technol. **6**, 468 (1997).
[8]R. H. Stark and K. H. Schoenback, J. Appl. Phys. **85**, 2075 (1999).
[9]K. Schoenbach, A. El-Habachi, M. Moselhy, W. Shi, and R. Stark, Phys. Plasma **7**, 2186 (2000).
[10]J. Kolb, A. Mohamed, R. Price, J. Swanson, A. Bowman, R. Chiavarini, M. Stacey, and K. Schoenbach, Appl. Phys. Lett. **92**, 241501 (2008).
[11]D. D. Hsu and D. B. Graves, Plasma Chem. Plasma Process. **25**, 1 (2005).
[12]H. Qiu, K. Martus, W. Y. Lee, and K. Becker, Int. J. Mass Spectrom. **233**, 19 (2004).
[13]C. Penache, M. Miclea, A. Bräuning-Demian, O. Hohn, S. Schössler, T. Jahnke, K. Niemax, and H. Schmidt-Böcking, Plasma Sources Sci. Technol. **11**, 476 (2002).
[14]Dj. Spasojević, M. Cvejić, N. M. Šišović, and N. Konjević, Appl. Phys. Lett. **96**, 241501 (2010).
[15]P S. Kothnur and L. L. Raja, J. Appl. Phys. **97**, 043305 (2005).
[16]H. Nojima, R.-E. Park, J.-H. Kwon, I. Suh, J. Jeon, E. Ha, H.-K. On H.-R. Kim, K. Choi, K.-H. Lee, B-L. Seong, H. Jung, S. J. Kang, S. Namba, and K. Takiyama, J. Phys. D: Appl. Phys. **40**, 501 (2007).
[17]R.W.P. McWhirter, in *Plasma Diagnostic Techniques*, edited by R. H. Huddlestone and S. L. Leonard (Academic, New York, 1965).
[18]N. Konjević, Phys. Rep. **316**, 339 (1999).
[19]S. Djurović and N. Konjević, Plasma Sources Sci. Technol. **18**, 035011 (2009).
[20]H. R. Griem, *Spectral Line Broadening by Plasmas* (Academic, New York, 1974).
[21]H. R. Griem, *Plasma Spectroscopy* (McGraw-Hill, New York, 1964).
[22]M A. Gigosos, M. Á. González, and V. Cardeñoso, Spectrachimica Acta Part B **58**, 1489 (2003).
[23]C. Stehle and R. Huucheon, Astron. Astrophys. Suppl. Ser. **140**, 93 (1999).
[24]M. Miclea, K. Kunze, U. Heitmann, S. Florek, J. Franzke, and K. Niemax, J. Phys. D, Appl. Phys. **38**, 1709 (2005).
[25]J. Luque and D. R. Crosley, "LIFBASE" Database and Spectral Simulation Program (Version 1.9), SRI International Report No. Mp 99-009, 1999.